Arab J Geosci (2017) 10: 356
DOI 10.1007/s12517-017-3141-7

ORIGINAL PAPER

Reconstruction of Indian monsoon precipitation variability between 4.0 and 1.6 ka BP using speleothem $\delta^{18}O$ records from the Central Lesser Himalaya, India

Lalit M. Joshi[1] · Bahadur Singh Kotlia[1] · S. M. Ahmad[2] · C.-C. Wu[3] · Jaishri Sanwal[4] · Waseem Raza[2] · Anoop K. Singh[1] · C.-C. Shen[3] · Tengwen Long[5] · Arun K. Sharma[1]

Received: 4 December 2016 / Accepted: 4 August 2017 / Published online: 14 August 2017

Abstract The present study documents the monsoon precipitation variability spanned ~ 2500 years, between 4.0 and 1.6 ka BP (before 1950 AD), from the Central Lesser Himalaya, India, using $\delta^{18}O$ measurements of Tityana cave stalagmite (hereafter referred as TC1). At present, the cave receives precipitation from both Indian Summer Monsoon (ISM) and Western Disturbances (WDs). The $\delta^{18}O$ variation between − 8.04 and − 10.46‰ through growth axis of the TC1 and five ^{14}C AMS dates (due to large age uncertainty by $^{230}Th/U$ method) have allowed us to identify the mid to late Holocene multi-decadal to centennial scale climatic oscillations. The higher $\delta^{18}O$ values indicate the weakening of the monsoon precipitation, while the lighter values represent the stronger monsoon precipitation strength. Based on the fluctuations in $\delta^{18}O$ values, three distinct phases of the precipitation variability are distinguished as, declined/decreased precipitation between ~ 4.0 and 3.4 ka BP with peak aridity around ~ 3.4 ka BP, followed by slightly improved conditions from ~ 3.4 to ~ 2.7 ka BP. Subsequently, the climate was reduced from ~ 2.7 ka BP onwards until the end of stalagmite growth, around ~ 1.6 ka BP with spikes of two major drought events centred at ~ 1.9 and ~ 1.6 ka BP. In general, the droughts, centred at ~ 3.4, ~ 1.9 and ~ 1.6 ka BP, are characterized by abrupt drop (from − 8.12 to − 8.04‰) in the $\delta^{18}O$ values and point to the weakening of the monsoon. One of the major drought events at ~ 3.4 ka BP can be correlated with the collapse of the Indus valley civilization in the NW India. A close correspondence of the TC1 data set with other WDs influenced regimes likely indicates a relative impact of mid-latitude WDs after transition of the mid-late Holocene around 3.5–3.4 ka BP.

Keywords Tityana cave (TC1) · $\delta^{18}O$ · ^{14}C AMS dating · Indian Summer Monsoon (ISM) · Western Disturbances (WDs) · Central Lesser Himalaya

Introduction

The monsoon variability in the Indian subcontinent is regulated by coupled heating-cooling between the Himalaya and southern Indian Ocean (Webster 1987; Webster et al. 1998; Chauhan 2003; Rehfeld et al. 2012; Gupta et al. 2013). The climate in Indian Himalaya is characterized by three monsoon patterns (Fig. 1), e.g. (i) Indian Summer Monsoon (ISM) or Southwest (SW) monsoon which brings rain over Indian subcontinent during June to September; (ii) Western Disturbances (WDs) which bring winter rains (from October to May) and play significant role over the northwestern India (Kotlia et al. 2012, 2015, 2017; Liang et al. 2015); and (iii) northeastern (NE) monsoon winds carry winter rains to southern part of the country during October to December; thus, there are diverse precipitation regimes from east to west. From the beginning of the Holocene (~ 11.7 ka BP onwards), the Himalaya

✉ Lalit M. Joshi
joshilalit81@gmail.com

[1] Centre of Advanced Study in Geology, Kumaun University, Nainital 263002, India

[2] CSIR-National Geophysical Research Institute, Hyderabad 500007, India

[3] High-Precision Mass Spectrometry and Environment Change Laboratory (HISPEC), Department of Geosciences, National Taiwan University, Taipei, Taiwan, Republic of China 10617

[4] Jawaharlal Nehru Centre for Advanced Scientific Research, Bangalore, India

[5] Section Palaeontology, Institute of Geological Sciences, Free University of Berlin, Berlin, Germany

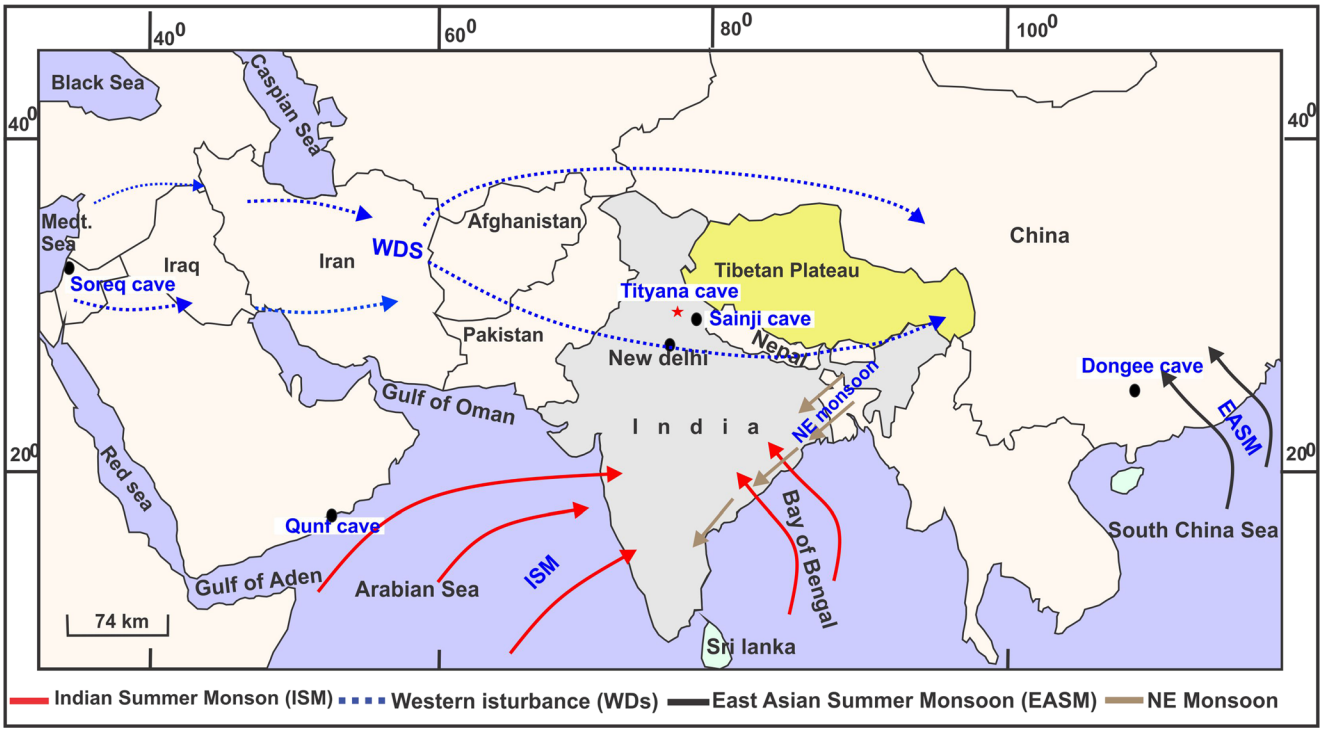

Fig. 1 Location of Tityana cave (TC1, present study) with trend of different monsoon system (ISM/EASM) and speculation of Winter Jet stream (WDs), split into two parts north and south of the Tibetan Plateau. Location of the caves of different precipitation regimes, e.g. Dongee cave (Dykoski et al. 2005); Sainji cave (Kotlia et al. 2015); Qunf cave (Fleitmann et al. 2007); Soreq cave (Bar-Matthews et al. 2003) to compare with TC1 paleo-precipitation record

underwent several wet and dry periods (Phadtare 2000; Kotlia et al. 2010). Earlier observations provoked that the monsoon intensity was weakened during the cold/dry events, i.e. Last Glacial Maximum (LGM), Older Dryas (OD), Younger Dryas (YD), 8.2 ka BP, 4.2 ka BP and Little Ice Age (LIA) (Sinha et al. 2005; Kotlia et al. 2010, Gupta et al. 2013). The homogeneous Indian monthly rainfall data during 1970–2000 shows several pulses of strengthening and failure of ISM, causing droughts and floods (Pant 2003). Variations in monsoon intensity and droughts have widespread socio-economic impacts over Indian subcontinent (Joseph et al. 2009; Kotlia et al. 2015). On the other hand, the Westerlies/Western Disturbances (WDs), originating from Mediterranean/North Atlantic Ocean, are also the important sources of rainfall for northwest India. The WDs have mechanical effect on atmospheric circulation, particularly during the winters when the winter jet streams carry moisture and blow from west to east and split into two parts, north and south of the Tibetan Plateau (Liang et al. 2015; Fig. 1), and prevent the southward flow of cold continental air towards the Indian subcontinent (Benn and Owen 1998).

The high-resolution short-term climatic events from the Central Himalayan domain between mid and late Holocene are either less understood or scattered. Prior to instrumental records, one needs to understand the past monsoon variability using high-resolution archives although a few palaeoclimatic records using continental archives (palaeolakes, peat bogs, modern lake sediments, etc.) from the Indian Himalaya are available (e.g. Kotlia et al. 1997, 2010; Phadtare 2000; Rühland et al. 2006; Kotlia and Joshi 2013; Demske et al. 2016), but the multi-centennial scale resolution and coarser sampling interval with age uncertainty offer only limited palaeoclimate information.

Stalagmites are one of the best continental archives which involve the deposition of calcium carbonate over long periods of time with decadal to century scale resolution and absolutely dated time series of the palaeoenvironmental variables (Fleitmann et al. 2007; Kotlia et al. 2012, 2015; Laskar et al. 2013). $\delta^{18}O$ variations in the speleothems can reflect the changes in isotopic composition of cave water which is directly related to the rainfall amount (Bar-Matthews et al. 1999) and is known as "amount effect" (Dansgaard 1964; Rozanski et al. 1992; Fleitmann et al. 2004; Sinha et al. 2005; Kotlia et al. 2012, 2015). Therefore, $\delta^{18}O$ and $\delta^{13}C$ variations in the stalagmites can be used to infer the palaeoclimatic reconstruction (Bar-Matthews et al. 1999) with low values (more negative) reflect higher amount of rainfall and vice versa (Burns et al. 1998, 2001, 2003; Neff et al. 2001; Fleitmann et al. 2004).

A few stalagmite $\delta^{18}O$-based palaeoclimatic records have been obtained from the Lesser Himalaya, e.g. Bølling-Ållerød interstadial between 15.2 and 11.7 ka from the Timta cave

(Sinha et al. 2005), the last ~ 400 years from the Chulerasim cave (Kotlia et al. 2012; Duan et al. 2013) and two millennia records from the Dharamjali cave (Sanwal et al. 2013) as well as from the Sahiya cave (Sinha et al. 2015), the last ~ 4 ka BP record from the Sainji cave (Kotlia et al. 2015) and 750 years records from the Panigarh cave (Liang et al. 2015). Most of these speleothems-based $\delta^{18}O$ records have documented not only the ISM variability but also highlighted the role of the WDs over the northwestern Himalaya during the late Holocene. Beyond the Himalayan records, a few speleothems $\delta^{18}O$ records are also available from the Peninsular India (Yadava and Ramesh 2005; Yadava et al. 2004; Sinha et al. 2007; Laskar et al. 2013; Lone et al. 2014; Raza et al. 2017). However, existing speleothems records between mid and late Holocene from the ISM/ASM and WDs domains such as Qunf cave, Oman (Fleitmann et al. 2007), Sainji cave, Central Himalaya (Kotlia et al. 2015), Dongge cave, China (Dykoski et al. 2005) and Soreq cave, Mediterranean/black sea regions (Bar-Matthews et al. 2003) are also discussed in text to compare our TC1 record. The present study from the central part of the Lesser Himalaya can extend our understanding of the behaviour of both source regions, e.g. ISM and WDs between ~ 4.0 and ~ 1.6 ka BP.

Study area, cave details and climatic perspectives

The Tityana cave (30° 38′ 30.7″ N, 77° 39′ 07.4″ E, altitude 1470 m; (Fig. 1) is located in the Deoban limestone of Precambrian age (Thakur and Rawat 1992), more precisely Mesoproterozoic or mid-late Riphean (Bhargava et al. 2011). The length of the cave is about 13 m with entrance diameter of 3 m × 1 m. The cave surface is undulated and has few subchambers. Presently, the cave is dry and has flowstones, stalactites and unbroken stalagmites. We collected a stalagmite sample at a distance of 12.1 m from the entrance in March, 2013, when the cave air temperature was about 22 °C with relative humidity inside the cave as 86% and 53% at cave ventilation. The surrounding vegetation is dominated by *Pinus* vegetation along with shrubs. The mean annual temperature of the area is between 22 and 25 °C with average annual precipitation of about 290 cm. Presently, the area receives 80% rainfall during summer season (June to September) and the remaining 20% is contributed by the WDs (October to May). The mean annual precipitation and temperature data for the past 43 years (1951–1995) at the nearest meteorological station of Dharamsala (www.imd.gov.in) are used in the present study (see Fig. 2). The station received the highest precipitation in 1958 (around 472 cm) and lowest in 1965 (161 cm) since the beginning of the instrumental records (see Fig. 2). There are also examples that the ISM clubbed with WDs and has created disastrous flood hazards in the neighbouring areas (Joshi and Kotlia 2015; Ray et al. 2016; Indian Disaster Report 2013).

Material and analytical procedures

The stalagmite was cut into two halves and gently polished using emery paper. Initially, the Hendy test was performed to recognize if the stalagmite was grown under the isotopic equilibrium (Hendy 1971). To test this hypothesis, we used two different layers from centre to right at 1.7 cm (layer 1) and 6.9 cm (layer 2) from the top. The Hendy test was performed at National Geophysical Research Institute, Hyderabad, India. Simultaneously, four samples (at 0–1, 47–48, 50–51 and 126–127 mm from the top) were analysed at Mass Spectrometry and Environmental Change Laboratory, National Taiwan University for $^{230}Th/U$ dating. The samples were analysed using multi-collector inductively coupled plasma mass spectrometer (MC-ICP-MS), following a standard procedure in Shen et al. (2003, 2012). An additional set of five samples (from depths at 0–1, 30–31, 63–64, 93–94, 127–128 mm), were sent to Poznan Radiocarbon Laboratory for ^{14}C AMS dating. The OxCal v.4.2 software package (after Bronk Ramsey 1995, 2001) was used to calibrate ^{14}C determination into calendar years and to model the age-depth relationship through a Poisson process depositional model (Bronk Ramsey 2008). This model allows flexible change in sedimentary rate and proves effective in simulating growth of speleothems (Scholz et al. 2012). We set up the critical values as 68 and 95%, respectively, for agreement index and convergence index in the model (Bronk Ramsey 1995).

A total of 130 samples (in addition to the Hendy test) were milled at an interval of 1 mm along its central growth axis for $\delta^{18}O$ measurement using a micro-driller (MANIX-180). All the measurements were done at National Geophysical Research Institute, Hyderabad, India, using a Delta Plus Advantage isotope ratio mass spectrometer (IRMS) coupled with a Kiel-IV automatic carbonate device. IAEA standard NBS-18 and NBS-19 were used to express the sample $\delta^{13}C$ and $\delta^{18}O$ values with respect to Vienna Pee Dee Belemnite (VPDB) standard. The analytical precision was better than 0.1‰ for $\delta^{13}C$ and $\delta^{18}O$ (Ahmad et al. 2008). The VPDB standards were used for all isotopic compositions with analytical precision better than 0.10‰.

For mineralogy, 1 g powder was drilled with a 1-mm drill bit from different darker and lighter layers of TC1 at various depths using the micro-driller (NICRAFT MB-130). The mineralogical composition was analysed using Philips single crystal X-ray diffractometer with CCD facility (Siemens). X-ray diffraction (XRD) pattern has recorded 2θ position ranges at 10–80°. Further, three thin sections (3 × 3 cm) and ten stubs (~ 0.5 cm) were prepared for petrography under scanning electron microscope (SEM). The composition of stalagmite

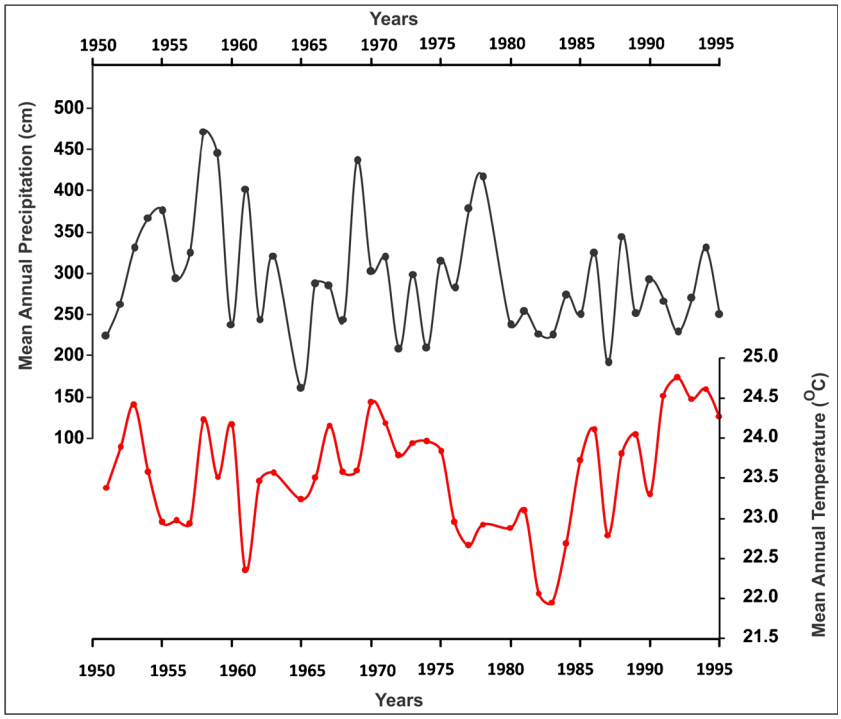

Fig. 2 Temperature and precipitation data of past 44 years (during 1951–1995) from the nearest meteorological station at Dhramsala (Source: www.imd.gov.in)

identified using energy dispersive X-ray analyser (EDS, Cambridge). The XRD and SEM analysis were carried out at Jawaharlal Nehru Centre for Advance Scientific Research (JNCASR), Bangalore, India.

Results and discussion

Hendy test

Hendy (1971) suggested that $\delta^{18}O$ and $\delta^{13}C$ values remain constant along a single growth layers if the sample was formed under the isotopic equilibrium. In the case of TC1, a small shift is observed in $\delta^{18}O$ and $\delta^{13}C$ values along layer 1 (Fig. 3a) which may be due to shifting of the drill bit while milling the sample. However, the low (0.042) correlation coefficient (r^2) between $\delta^{18}O$ and $\delta^{13}C$ suggests sufficiently slow degassing of CO_2 to maintain the isotopic equilibrium during carbonate precipitation. For layer 2, the $\delta^{18}O$ and $\delta^{13}C$ values remains are constant (Fig. 3a). The Hendy test was further checked through the correlation between all the values of $\delta^{18}O$ and $\delta^{13}C$ (Fig. 3b) and the low r^2 (0.19) indicates that the kinetic fractionation was negligible (Fig. 3); hence, the $\delta^{18}O$ in the sample may well reflect the climate signal. Besides, more recent studies have argued over the Hendy test and advocated the reliability of $\delta^{18}O$ signal in the stalagmite despite the failure of the test (Fleitmann et al. 2004; Dorale and Liu 2009; Zhou et al. 2011; Kotlia et al. 2012)

Chronology and age-depth relationship

The $^{230}Th/U$ dating of TC1 stalagmite was unsuccessful due to multiple sources of non-authigenic ^{232}Th and low uranium concentration (< 10 ppb) (Table 1). The high content of thorium appears unlikely a product of the decay of ^{234}U in the sequence but more detrital or allogenic in origin (e.g. Blyth et al. 2017). The activity of detrital ^{230}Th seems not produced from the decay of ^{234}U due to high contribution of ^{232}Th from recrystallization of rock or may be allogenic transported from the nearby area through water and wind activity during leaching of the calcium carbonate and causing high uncertainty in $^{230}Th/^{232}Th$. The precision of the $^{230}Th/U$ dating strongly depends on the concentrations of uranium and detrital thorium (Goslar et al. 2000) and such a problem is not uncommon in using uranium-series method to date impure carbonates (e.g. Garnett et al. 2004; Durand et al. 2016) and in fact excludes a great amount of stalagmites, sometimes across a large geographical region, from being applicable in palaeoenvironmental reconstruction (Lechleitner et al. 2016).

The ^{14}C AMS dating is an alternative method to resolve the chronological issue of these stalagmites (Laskar et al. 2013; Zhao et al. 2015). Zhao et al. (2015) suggested that the younger ^{14}C AMS dates than $^{230}Th/U$ dates can reflect negligible dead carbon influence with strong influence of initial ^{230}Th in $^{230}Th/U$ ages. Therefore, the ^{14}C AMS method has successfully been applied to build chronologies for young speleothems (Goslar et al. 2000; Mattey et al. 2008; Laskar et al. 2013; Zhao et al. 2015). In the present study, ^{14}C AMS

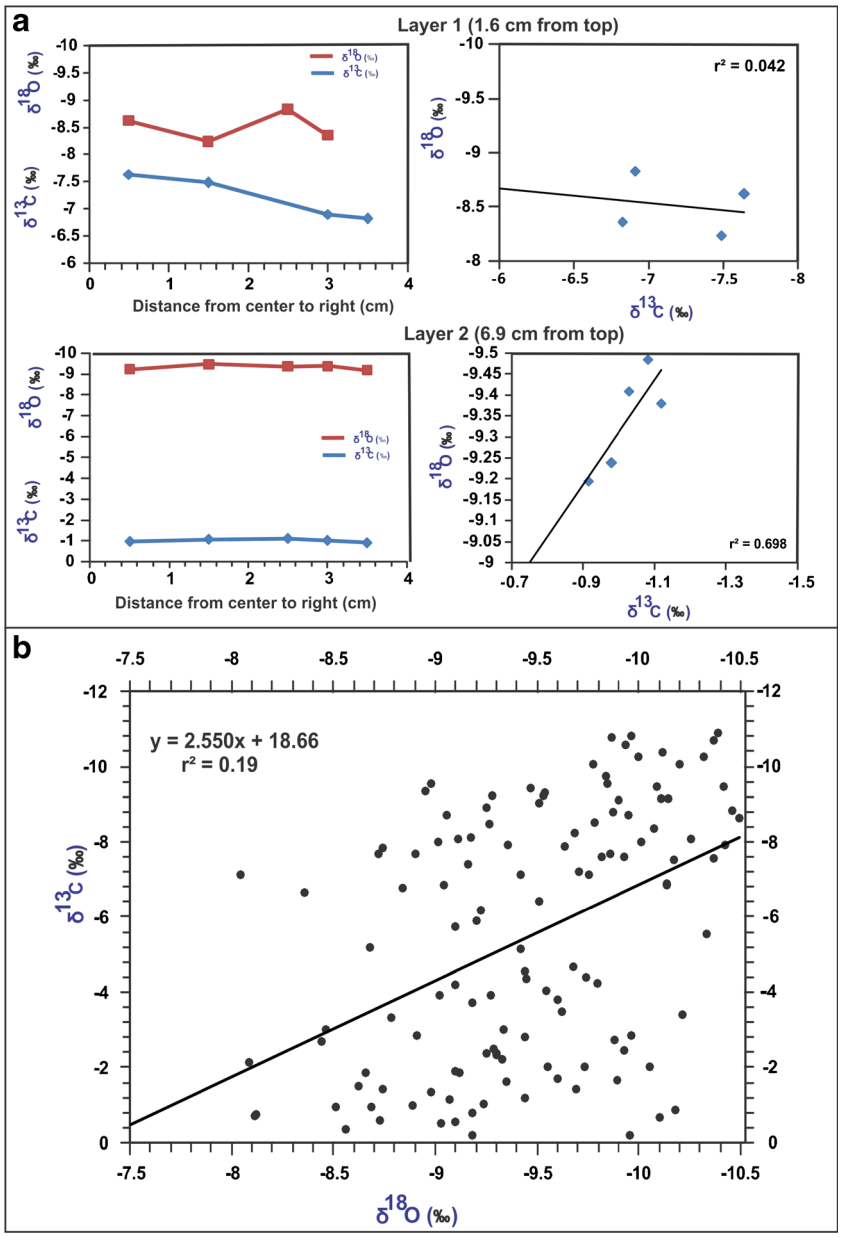

Fig. 3 **a** Hendy test for two layers of TC1 to indicate the kinetic equilibrium status. The results show the independent relationship between both $\delta^{13}C$ and $\delta^{18}O$ isotopes. The right panel shows the correlation between both $\delta^{13}C$ and $\delta^{18}O$ isotopes. **b** $\delta^{13}C$ and $\delta^{18}O$ plot of all isotopic data of TC1 along centre growth axis for further checking the kinetic fractionation. The plot also show the poor correlation between $\delta^{13}C$ and $\delta^{18}O$ ($r^2 = 0.19$)

dates are much younger than the ^{230}Th/U dates and possibly suitable for palaeoclimatic reconstruction (see Tables 1-2). We used five calibrated ^{14}C AMS dates to build TC1 chronology (Table 2).

The five ^{14}C AMS dates are in the stratigraphic order and thus provide a reasonable basis for establishing the age-depth relationship (Fig. 4a). However, carbonate-related sediments are often strongly affected by ^{14}C reservoir effect because of carbon isotopic signals introduced from the ^{14}C-depleted bedrock (Genty et al. 2001; Hercman and Goslar 2002). Correction that removes the effect was therefore necessary to estimate precise radiocarbon ages. The dead carbon fraction (DCF) correction (after Hua et al. 2012) was performed in order to infer contemporaneous atmospheric ^{14}C content from the measured ^{14}C radioactivity. However, estimating the DCF in the TC1 sample proved challenging because of the lack of suitable anchor points that could be reliably dated by other radiometric methods. Furthermore, according to field observations, the growth of the stalagmite might have ceased for a long time and the top of the sample was not likely modern in age (cf. Li et al. 1996). Dead carbon correction remains a major difficulty in dating cave sediments, not only because it is not always feasible to find an independent dating series to correct the reservoir effect, but also because of the high level of variability of dead carbon contents across space and through time (Lechleitner et al. 2016). A well-recognized approach is to assume a more or less averaged, constant DCF throughout studied speleothems (see Reimer et al. 2013). In

Table 1 The ^{230}Th/U date of TC1 stalagmite. The instrumental analysis on MC-ICP-MS (after Shen et al. 2003; Shen et al. 2012). Analytical errors is 2 s of the mean

Depth from top (mm)	^{238}U ppb[a]	^{232}Th ppt	$d^{234}U$ measured[a]	[^{230}Th/^{238}U] activity[c]	[^{230}Th/^{232}Th] ppm[d]	Age uncorrected	Age corrected[c,e]	$d^{234}U_{initial}$ corrected[b]
0–1	97.00 ± 0.10	94,916 ± 795	39.5 ± 2.0	0.231 ± 0.022	3.89 ± 0.38	27,379 ± 3025	− 846 ± 16,432	39.4 ± 2.6
47–48	136.98 ± 0.42	134,334 ± 1607	27.2 ± 9.5	0.2210 ± 0.0174	3.72 ± 0.30	26,390 ± 2372	− 2312 ± 16,671	27.0 ± 9.5
50–51	84.54 ± 0.20	45,903 ± 262	24.8 ± 3.2	0.2606 ± 0.0100	7.91 ± 0.31	31,963 ± 1426	16,987 ± 8142	26.0 ± 3.4
126–127	171.00 ± 0.24	46,516 ± 272	22.2 ± 1.8	0.1430 ± 0.0041	8.67 ± 0.25	16,420 ± 507	9149 ± 3792	22.8 ± 1.8

[a] $[^{238}U] = [^{235}U] \times 137.818$ (± 0.65‰) $d^{234}U = ([^{234}U/^{238}U]_{activity} - 1) \times 1000$

[b] $d^{234}U_{initial}$ corrected was calculated based on ^{230}Th age (T), i.e. $d^{234}U_{initial} = d^{234}U_{measured} X e^{l234 \times T}$, and T is corrected age

[c] $[^{230}Th/^{238}U]_{activity} = 1 - e^{-l230T} + (d^{234}U_{measured}/1000)[l_{230}/(l_{230} - l_{234})](1 - e^{-(l230 - l234)T})$, where T is the age. Decay constants are 9.1705×10^{-6} years^{-1} for ^{230}Th, 2.8221×10^{-6} years^{-1} for ^{234}U (Cheng et al. 2012) and 1.55125×10^{-10} years^{-1} for ^{238}U (Jaffey et al. 1971)

[d] The degree of detrital ^{230}Th contamination is indicated by the [^{230}Th/^{232}Th] atomic ratio instead of the activity ratio

[e] Age corrections for samples were calculated using an estimated atomic ^{230}Th/^{232}Th ratio of 4 ± 2 ppm

Those are the values for a material at secular equilibrium, with the crustal ^{232}Th/^{238}U value of 3.8. The errors are arbitrarily assumed to be 50%

the TC1, we tentatively assumed a constant DCF value of ~ 15%, although hypothetical, as has been done in other studies (e.g. Genty and Massault 1997; Genty et al. 2001) and an observation that an age difference of ~ 1000–1500 years due to dead carbon is most commonly encountered (Laskar et al. 2011). Although limitations associated with this hypothetical DCF need to be treated with caution when interpreting the data, a good correlation between the TC1 sample and other palaeoclimatic records from nearby areas appears to strengthen the reasonability of our correction.

The radiocarbon measurements are reported in terms of years BP (reference year is 1950 AD). The linear regression lines of calibrated ^{14}C AMS ages have r^2 value about 0.93 (Fig. 4a). The Poisson process depositional model incorporates these corrected radiocarbon dates as shown in Fig. 4b. All agreement indexes and convergence indexes in the model were higher than the default critical values, thus validated the model. The model was set with critical values 95% confidence level and median dates were used for further extrapolation. According to the age-depth relationship, the TC1 stalagmite seems to have deposited between ca. 4.0 ka BP and 1.6 cal ka BP.

Mineralogy and petrography

The powder XRD technique and EDS reveal that the stalagmite is made up of calcite (Fig. 5a, b). The SEM images indicate that it is mostly composed of laminated compact calcite with two thin porous layers at 0.8- and 1.8-cm depth (Fig. 6a). Sometimes, the crystallization is between palisade calcite (PC) and columnar calcite (CC). The CC crystals at 0.5, 3.5 and 8–8.5 cm (Fig. 6b–d) and the PC crystals at 2–2.5 and 7–7.5 cm are observed (Fig. 6e, f) and a multiple growth of small PC and equant calcite (EC) are viewed at 10.5–11 cm (Fig. 6g). The CC crystals are elongated with orientated crystallographic axis is parallel to the earlier growth surface (Fig. 6b–d) and may have been formed either by direct precipitation or as a recrystallization product of precursor aragonite (e.g. Perrin et al. 2014). In subtropical climates, calcite crystallization is favoured during the wet season because of higher cave humidity (Denniston et al. 2000). The palisade calcite (PC) shows growth direction parallel to the crystal boundaries (Fig. 6e, f). Large and well-developed crystals of equant calcite (EC) with multiple growth of

Table 2 ^{14}C activity (presented as pMC) of the ^{14}C dates from TC1 stalagmite and their calibrated age (in calendar years) after dead carbon correction

Sample code	Lab code	Depth (cm)	pMC (%, 1σ)	Uncorrected radiocarbon date (^{14}C bp, 1σ)	Corrected pMC[a] (%, 1σ)	Calibrated 95% range (cal BP)[b]	Calibrated median (cal BP)[b]
TCA_1	Poz-66853	0–1	69 ± 0.257	2985 ± 30	81.2 ± 0.257	1688–1531	1578
TCA_2	Poz-66854	30–31	64.9 ± 0.282	3475 ± 35	76.4 ± 0.282	2309–2063	2199
TCA_3	Poz-66855	63–64	57.3 ± 0.249	4470 ± 35	67.4 ± 0.249	3453–3344	3395
TCA_4	Poz-66856	93–94	56.1 ± 0.244	4640 ± 35	66.0 ± 0.244	3677–3479	3576
TCA_5	Poz-66857	127–128	54.1 ± 0.269	4940 ± 40	63.6 ± 0.269	4080–3844	3941

[a] The dead carbon correction followed the procedure by Hua et al. (2012), assuming a dead carbon fraction of ca. 15%

[b] Radiocarbon dates were calibrated in OxCal v.4.2 (Bronk Ramsey 1995) using the IntCal13 calibration curve (Reimer et al. 2013)

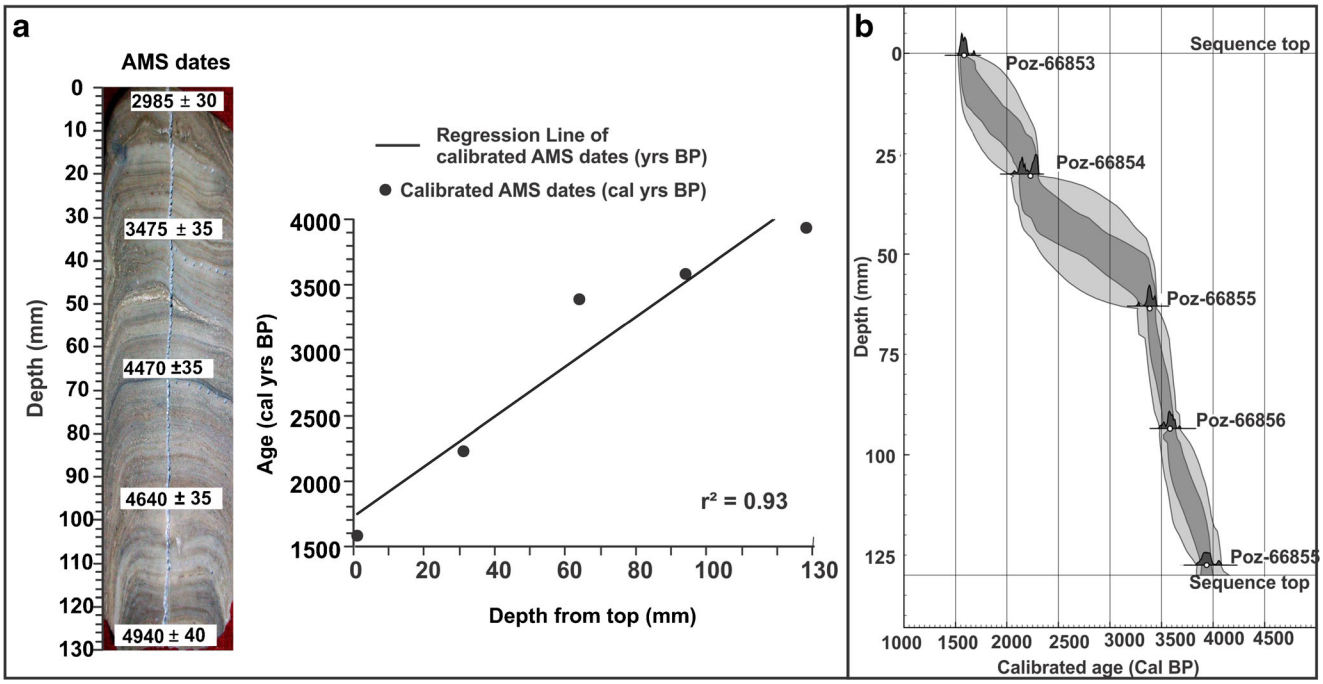

Fig. 4 **a** TC1 cave stalagmite sample and uncalibrated ^{14}C AMS dates and age-depth relationship with regression line have $r^2 = 0.93$. **b** TC1 stalagmite sequence and reconstructed age-depth relationship based on AMS ^{14}C dating. The wider and lighter shade represents 95% probability range, while the narrower and darker shade represents 68% probability range. The median of the probability distributions are indicated as open circles

small palisade are also observed (Fig. 6f) and they are closely packed and oriented parallel to each other (Fig. 6g). The cavities show the growth of small equant calcite towards the voids from the wall of stalagmite (Fig. 6g). Two thin porous EC layers are observed along the central growth axis at 5–5.5 and 9–9.5 cm (Fig. 6h). The boundary between the CC and EC layers is clearly visible with two small cavities (Fig. 6i).

Palaeoclimatic reconstruction using $\delta^{18}O$ and $\delta^{13}C$ variations

The long-term records of rainwater $\delta^{18}O$ concentration are not available from the northwest India. The only long-term record (1940–2004) of temperature, humidity and rainwater $\delta^{18}O$ measurements are available from Delhi Metrological station (GNIP; http://www.iaea.org/water) (Fig. 7a). The rainfall

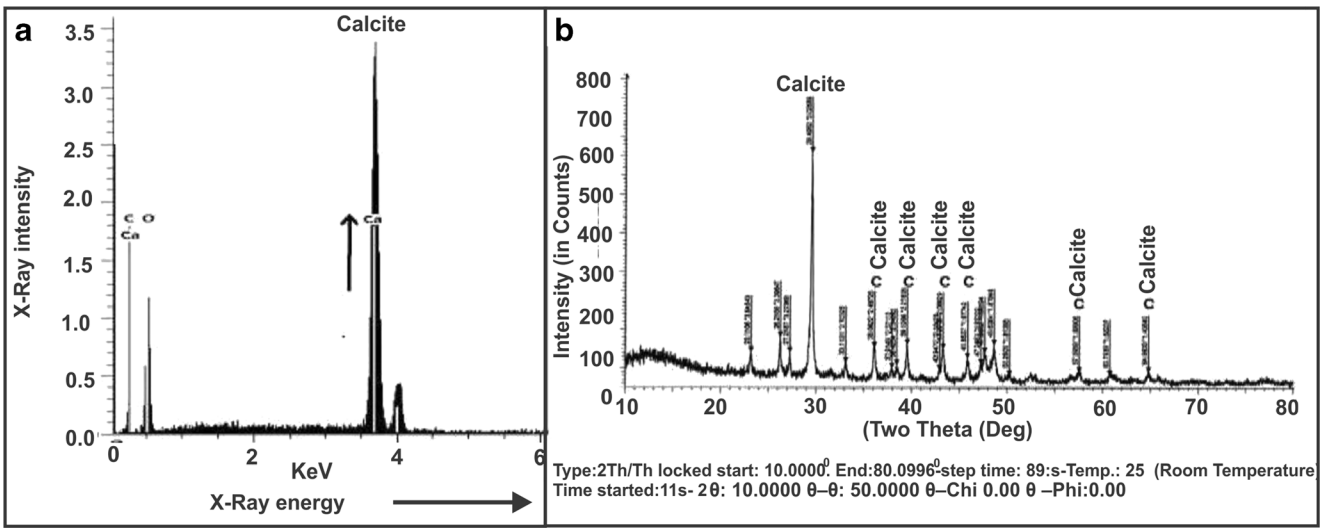

Fig. 5 **a** The representative graphs of energy dispersive X-ray analysis (EDS) in different depths. **b** The X-ray diffraction analysis (XRD) of TC1 from the various depths of stalagmite indicate that all are calcite peaks

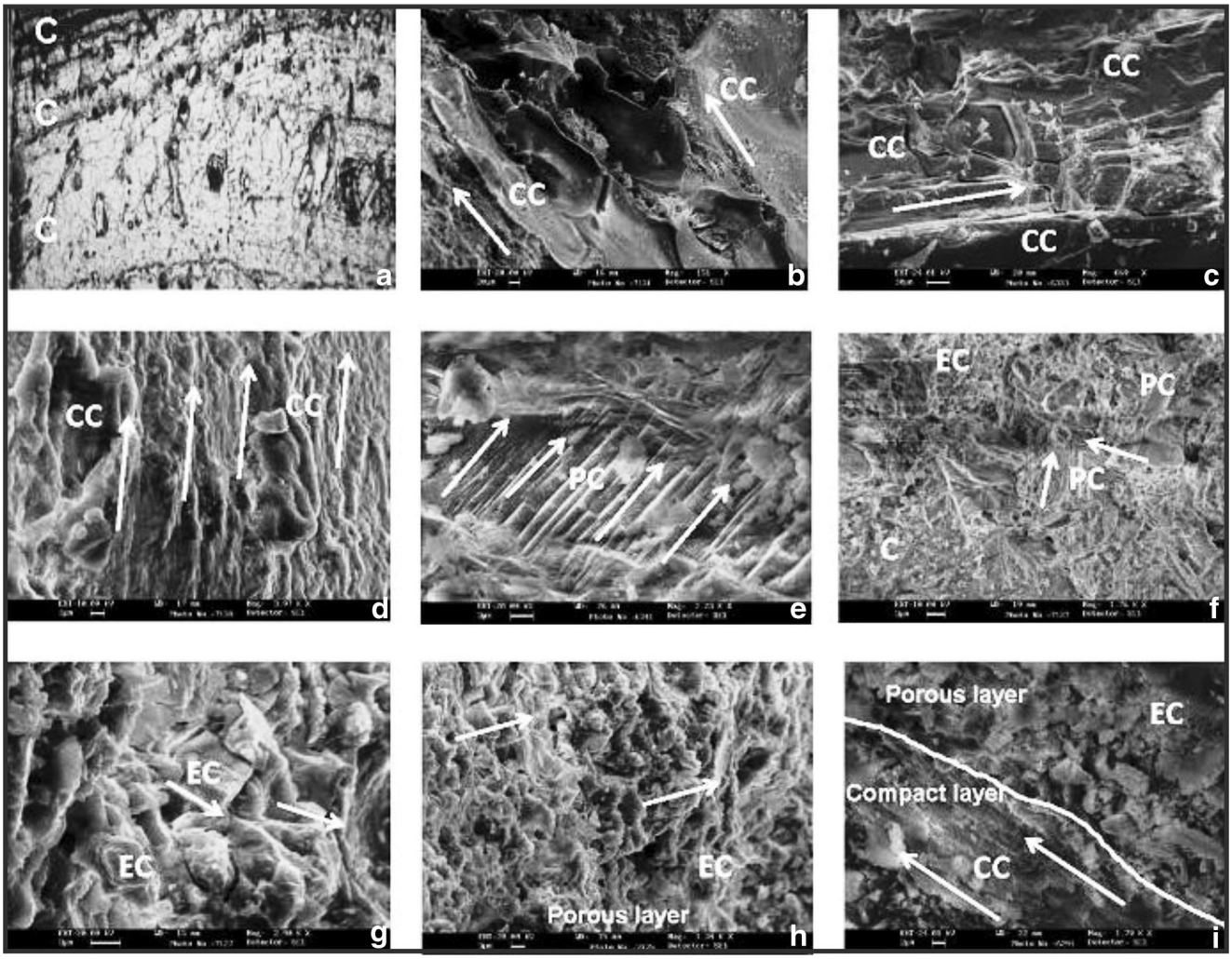

Fig. 6 The micrograph showing **a** the large elongated compact calcite crystals; **b** elongates columnar crystals of calcite with their orientation and termination; **c** orientation of large columnar calcite crystal; **d** parallel columnar calcite (CC) crystal radiating from the stalagmite growth direction; **e** straight parallel crystals of palisade calcite (PC); **f** Multiple growth of small palisade and equant calcite crystal; **g** closely packed and well-developed large equant calcite crystals showing inside growth with small cavity on stalagmite surface; **h** growth of numerous small crystals of equant calcite in porous layers; **i** the columnar and equant calcite along with the boundary between compact and porous layer. All the arrows are indicating the direction of crystal orientation

$\delta^{18}O$ values at New Delhi show that the precipitation during the ISM months (i.e. July–August–September) is characterized by lower $\delta^{18}O$ values, higher relative humidity and less temperature compared to restively hotter months (i.e. May–June) (Fig. 7a). Therefore, higher rainfall with higher humidity should lead to a minimum evaporation under reduced kinetic fractionation, thus maintaining the low $\delta^{18}O$ values (Kotlia et al. 2012, Fig. 7a). Nevertheless, New Delhi (average ISM $\delta^{18}O$ values as − 6.8‰; GNIP, http://www.iaea.org/water) and cave site have different elevation of ~ 1250 m and thus the $\delta^{18}O$ precipitation at TC1 is supposed to be about 3.6‰ lower compared to the New Delhi due to altitude effect as $\delta^{18}O$ values are lower with ~ 0.3‰/100 m towards higher elevations (Hren et al. 2009; Kotlia et al. 2015), resulting in − 10.4‰ around the cave site. However, the TC1 average $\delta^{18}O$ values are − 9.25‰, still higher than the expected values. Therefore, it appears that the TC1 was influenced not only by the ISM but also by another moisture source which could be ascribed to the WDs. It is important to note that the $\delta^{18}O$ isotopic composition is directly related to precipitation (Hern et al. 2009; Kumar et al. 2010; Kotlia et al. 2017).

Due to lack of rainfall $\delta^{18}O$ data from any nearby stations, we used 1-year data from Uttarkashi (Kumar et al. 2010) to understand the rainfall isotopic composition near the cave location (Fig. 7a, b). The data set (from − 0.8 to − 20.8‰) shows lower $\delta^{18}O$ values during ISM months (Fig. 7b). Therefore, the higher rainfall giving rise to depleted $\delta^{18}O$ values perhaps indicate the "amount effect" in precipitation (Gonfiantini et al. 2001; Kumar et al. 2010; Liang et al. 2015; Kotlia et al. 2017). Additionally, the $\delta^{18}O$ and $\delta^{2}H$ values have significant variations ($\delta^{2}H$ ranges from − 157 to + 14.1‰ and $\delta^{18}O$ ranges

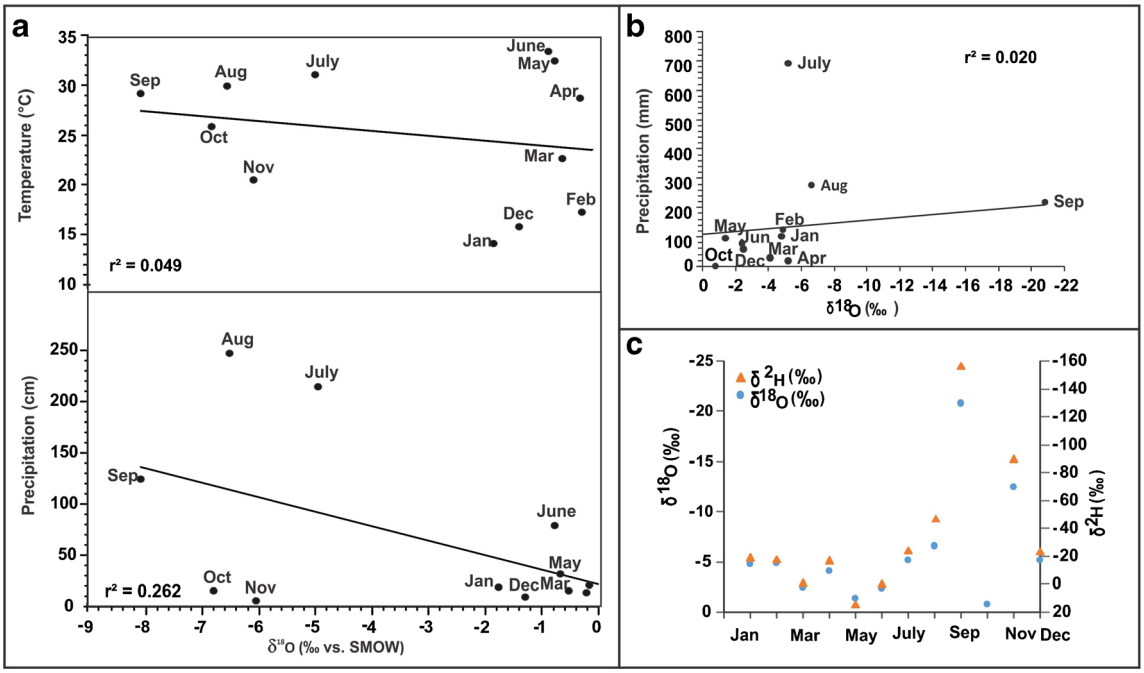

Fig. 7 **a** Rainfall $\delta^{18}O$ values and temperature data during 1960–2004 at New Delhi metrological station, indicating that the lower $\delta^{18}O$ associated with stronger monsoon precipitation and has relatively lower temperature than hotter month in northern India (May–June). **b** The GNIP precipitation vs $\delta^{18}O$ values for the year 2005 at Uttarkashi area (nearest to present cave location) also representing the higher rainfall and lighter $\delta^{18}O$ during monsoon months. **c** Lower $\delta^{18}O$ and $\delta^{2}H$ values for August–September and November indicates the contribution of WDs. In general, the higher rainfall related to more negative $\delta^{18}O$ suggest the amount effect

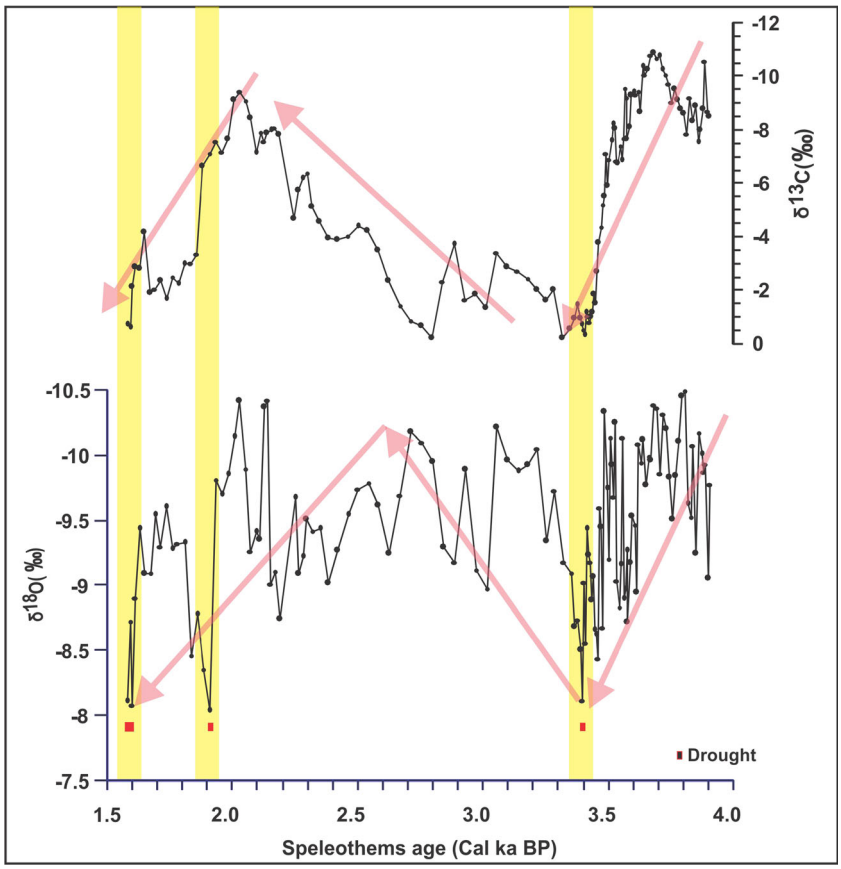

Fig. 8 $\delta^{18}O$ and $\delta^{13}C$ variation of TC1 with three distinct phases of past precipitation with major drought events centred at ~ 3.4, ~ 1.9 and ~ 1.6 ka BP. The vertical yellow panels show the drought period

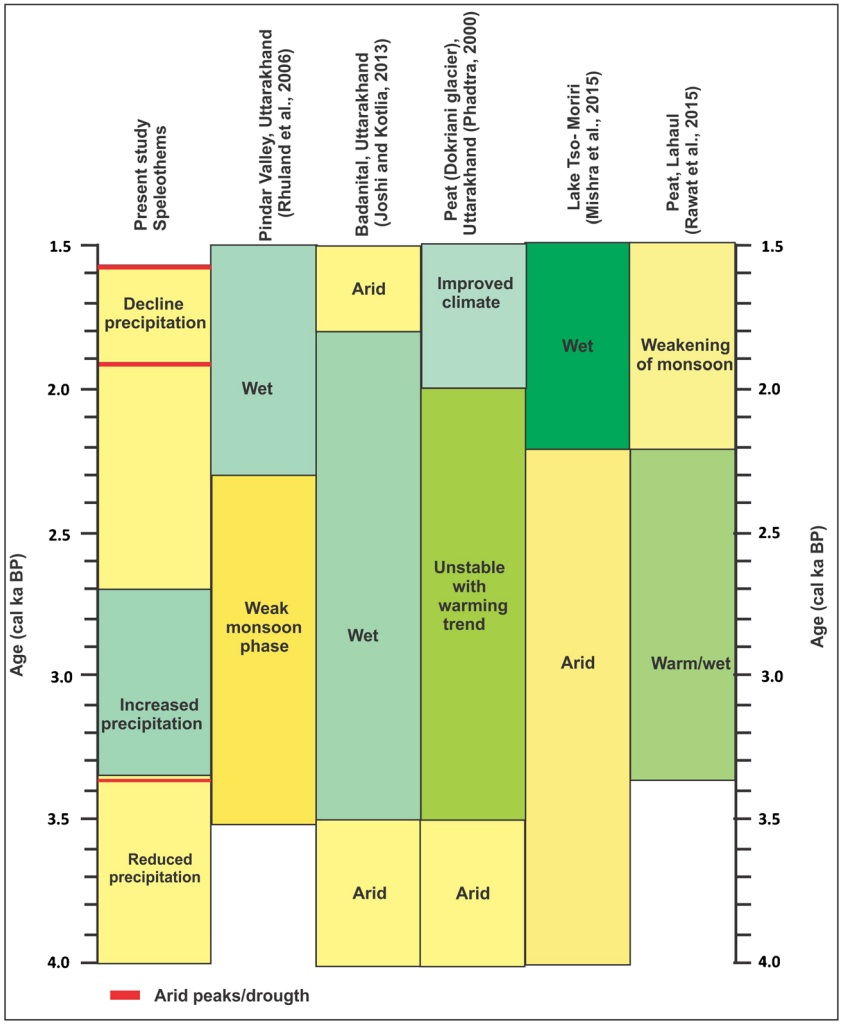

Fig. 9 Comparison of TC1 record with other records of NW Himalaya indicates a relative impact of WDs after transition of Mid-Late Holocene around 3.5–3.4 ka BP

from − 20.8 to − 0.8‰, respectively; Fig. 7c) due to amount effect and also possibly indicate contribution of the WDs (Kumar et al. 2010; Liang et al. 2015; Kotlia et al. 2015, 2017). Similarly, the $\delta^{18}O$ values at New Delhi for winter months (December–March) range between 0.2 and − 1.8‰ (Fig. 7a) while the values range from − 2 to − 6‰ for Uttarkashi locality for the same period (Fig. 7b), further indicating contribution of the WDs. A large variation in stalagmite $\delta^{18}O$ values of the northwest Himalayan sites compared to the ISM dominated caves has previously been attributed to the input of WDs (Kumar et al. 2010; Kotlia et al. 2015, 2017; Liang et al. 2015).

Stalagmite $\delta^{13}C$ primarily reflects vegetation cover and dense cover are generally characterized by low $\delta^{13}C$ values due to dissolving of more biogenic CO_2 into the seepage water (Kotlia et al. 2017). Contrary to this, stalagmite $\delta^{13}C$ values are higher due to less contribution of biogenic CO_2 under stressed climatic conditions (Kotlia et al. 2017). For palaeoclimatic reconstruction, use of $\delta^{13}C$ is based on widely differing $^{13}C/^{12}C$ ratios of the C_3 and C_4 plants. The C_3 and C_4 plants, separated on the basis of their photosynthesis pathways of carbon fixation have $\delta^{13}C$ values in the range of − 26 to − 28‰ (with a mean of − 26‰) and − 11 to − 14‰ (with a mean of − 12‰), respectively (Smith 1972; Smith and Epstein 1971). Thus, the lower $\delta^{13}C$ values under the C_3 vegetation should broadly indicate warmer/wetter conditions as the $\delta^{13}C$ values in cave speleothems depend on the CO_2 in the soil, fractionation and the extent of exchange between seepage drip water and host rock (Smith 1972; Smith and Epstein 1971; Kotlia et al. 2015). In the TC1, the $\delta^{13}C$ values are increased (from − 10.57 to − 0.19‰) with increasing aridity between ~ 4.0 and ~ 3.4 ka BP. The $\delta^{13}C$ values ere highest around ~ 3.4 ka BP, suggesting peak aridity. Thereafter, the values decrease from ~ 3.4 to 2.0 ka BP (0.19 to − 9.43‰), reflecting improved C_3 vegetation under favourable climatic conditions. The $\delta^{13}C$ values show positive relationship with $\delta^{18}O$ during the arid events around ~ 3.4, ~ 1.9 and ~ 1.6 ka BP,

Based on the $\delta^{18}O$ variations, the TC1 deposit is divided into three distinct climate zones: (1) reduced precipitation between ~ 4.0 and ~ 3.4 ka BP, characterized by enhancement in $\delta^{18}O$ values by about > − 1‰ (between − 9.78 and − 8.63 ‰) with abruptly higher $\delta^{18}O$ at ~ 3.4 ka BP (− 8.11‰) (see

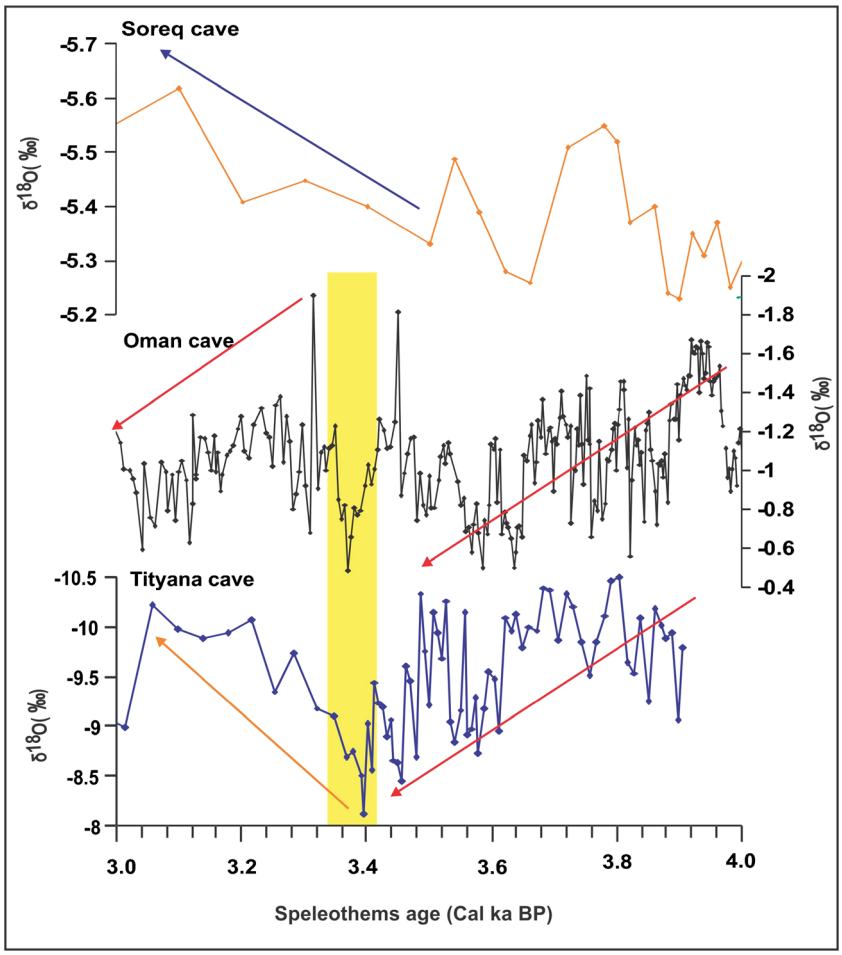

Fig. 10 Comparison of TC1 record between 4 and 3 ka BP with stalagmite records from ISM dominated Oman cave (Fleitmann et al. 2007) and WDs influenced Soreq cave (Bar-Matthews et al. 2003), suggesting the amount effect in TC1 due to two different moisture regime, e.g. WDs and ISM. The vertical yellow panels show the peak aridity around ~ 3.4 ka BP, which is well correlated with decline of Indus valley civilization. The Soreq cave and TC1 records show close correspondence, while Qunf cave show opposite trend

Fig. 8), (2) slightly improved and favourable climatic conditions between ~ 3.4 and 2.7 ka BP by depletion in $\delta^{18}O$ values for about > − 1.5‰ (− 8.63 to − 10.18‰; Fig. 8) and (3) arid conditions from ~ 2.7 ka BP onwards prevailing until 1.5 ka BP with enhancement in $\delta^{18}O$ values for about − 2‰ (− 10.18 to − 8.08‰; Fig. 8). Between ~ 2.7 and ~ 1.5 ka BP, two peak drought events were observed at ~ 1.9 ka BP (− 8.04‰) and ~ 1.6 ka BP (− 8.08‰) and are characterized by abrupt enhancement in $\delta^{18}O$ values (Fig. 8). Similar results have been obtained from the Sainji cave, Kumaun Himalaya (Kotlia et al. 2015) and Soreq cave, from eastern Mediterranean (Bar-Matthews et al. 2003).

Comparison with other records

The mid to late Holocene climatic records from northwest Himalaya are mainly from the modern lakes, palaeolakes and peat bogs, although some with coarse sampling interval (Fig. 9). In the TC1 data, an abrupt drop in $\delta^{18}O$ and $\delta^{13}C$ with peak aridity around ~ 3.5–3.4 ka BP correspond to the transition of mid to late Holocene. This event is prominent in almost all the records obtained from peat bogs and lake sediments and reflect weakening of the ISM (Phadtare 2000; Rühland et al. 2006; Kotlia and Joshi 2013; Mishra et al. 2015; Rawat et al. 2015). Thereafter, the records are sparse in NW Himalaya (Fig. 9). In general, well-dated lake records from Garhwal Himalaya (Kotlia and Joshi 2013) and peat record from Lahaul region (Himachal Pradesh) show similar climatic variability (see Fig. 9; Rawat et al. 2015). Other available continental and marine records of the past climatic variability from nearby regions (e.g. China and Tibet Plateau) can also be compared with the TC1 record and so also with the Soreq cave (Bar-Matthews et al. 2003), Sainji cave (Kotlia et al. 2015), Qunf cave (Oman; Fleitmann et al. 2007) and Dongge cave (Dykoski et al. 2005) to understand the potential of well-dated stalagmite $\delta^{18}O$ from the climatically sensitive Himalayan sites. As mentioned above, three distinct climatic phases are recognized in the TC1 and are discussed further from the view-point of comparison.

~ 4.0–3.4 ka BP (declined precipitation) Declined precipitation during this period in the TC1 with peak aridity at ~ 3.4 ka BP seems coherent with the reduced precipitation in the Soreq cave between 4.5 and 2.5 ka BP (Bar-Matthews et al. 2003) with higher $\delta^{18}O$ around 3.5 ka BP (Fig. 10). Reduced

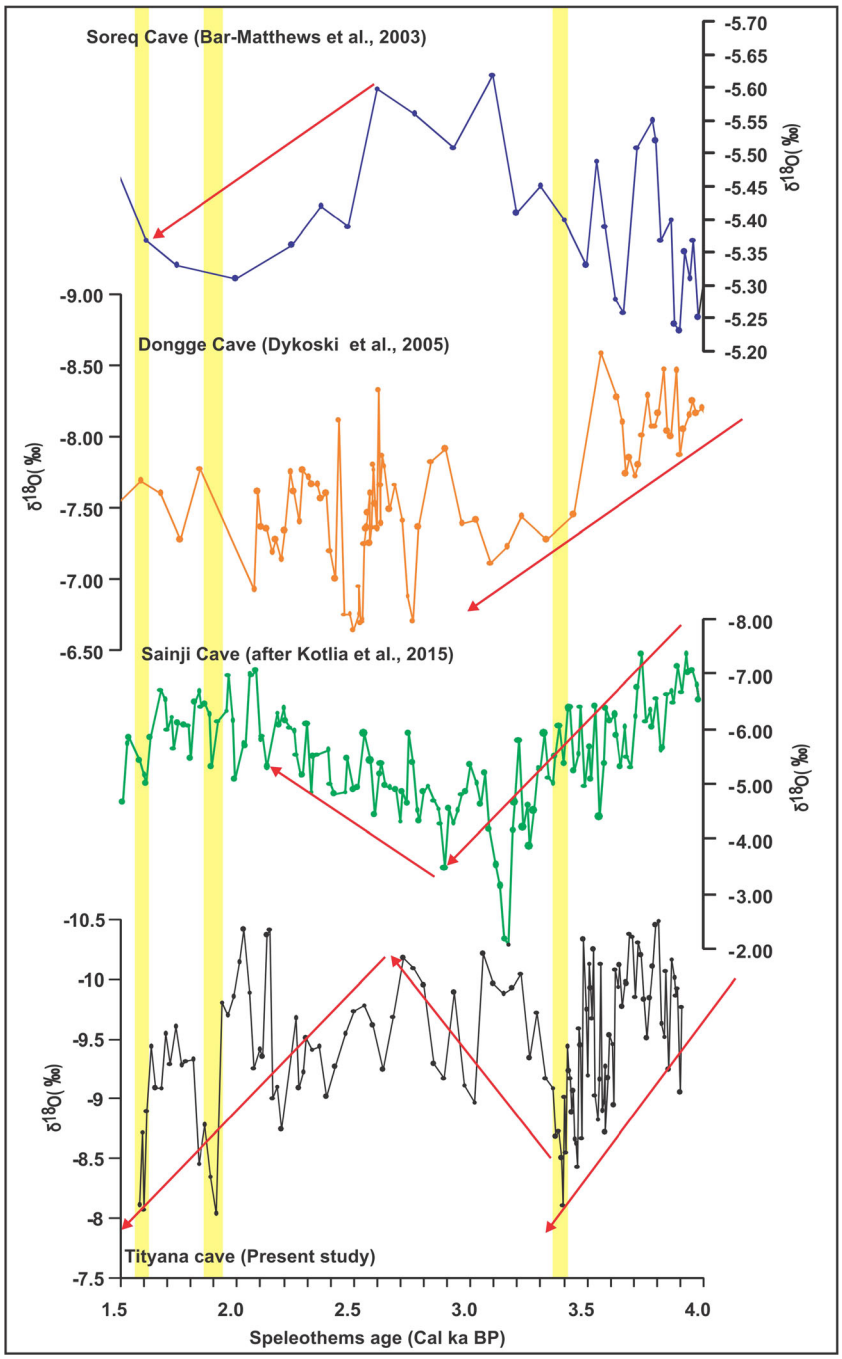

Fig. 11 Comparison of TC1 $\delta^{18}O$ record with stalagmite records from ISM and WDs dominated regimes, e.g. Qunf cave (Fleitmann et al. 2007); Dongge cave (Dykoski et al. 2005); Sainji cave (Kotlia et al. 2015) and Soreq cave (Bar-Matthews et al. 2003). The vertical panels show peak drought events. See Fig. 1 for the location of all the caves.

precipitation from ~ 4.0 to ~ 3.0 ka BP with the lowest precipitation at ~ 3.2 ka BP has also been observed in the Kumaun Himalaya (Kotlia et al. 2015). Within the period, similar fluctuations in $\delta^{18}O$ values were recognized in the Qunf cave with higher amplitude peak around 3.4 ka BP indicating weakened ISM (Fleitmann et al. 2007) (see Fig. 10). The declined intensity of monsoon at ~ 3.6 ka BP has also been registered in the Dongge cave records (Dykoski et al. 2005). Progressive lowering of lake took place in a northwest Himalayan lake around this time (Mishra et al. 2015) and the mean annual precipitation (MAP) reconstruction from the same lake confirms enhanced aridity between ~ 3.8 and 3.6 cal ka BP with markedly low lake level and less discharge in the River Indus around 3.2 ka BP (Leipe et al. 2014). The arid conditions between ~ 5.0 and 3.0 ka BP are also recorded from the Sanai lake in the Ganga plain, northern India (Sharma et al. 2004). Further, the lakes and peat records from the NW Himalaya also register intensification of aridity between ca. 4.0 and 3.5 ka BP (Chauhan and Sharma 1996; Kotlia et al. 1997; Phadtare 2000). The historical researches have also documented de-urbanization of the Indus valley culture at ~ 4.0 ka BP (Wright 2010; Dixit et al. 2014) and

the beginning of the collapse of Harappan civilization around 3.8 ka BP (Winner 2012) with its complete disappearance between ~ 3.5 and 3.0 ka BP (Leipe et al. 2014). A major dry spell from ~ 3.8 to 3.2 ka BP in the Bangong basin, (Gasse and Van Campo 1994) and significantly declined humidity in the Yunnan province around 3.4 ka BP (Xiao et al. 2014) may be positively correlated with our data set. Similarly, fall in the human civilization between 4.5 and 2.5 ka BP in the Middle East, North Africa and Egyptian kingdom (Hassan and Stucki 1987; Weiss et al. 1993; Bar-Matthews et al. 2003) confirm that this arid phase was experienced widely.

~ 3.4–2.7 ka BP (improved climatic conditions) In general, a gradual decrease in $\delta^{18}O$ values (− 8.63 to − 10.18‰) shows slightly favourable climatic conditions. Low $\delta^{18}O$ values between 3.2 and 2.0 ka BP are also documented from the Central Himalaya (Kotlia et al. 2015). However, the Dongge cave records are not coherent possibly due to low-resolution chronology in the TC1, while the Soreq cave data set shows similar fluctuations (Fig. 11). Pollen records from Lahaul, NW Himalaya indicate improved climatic conditions from ~ 3.4 to 2.0 ka BP (Rawat et al. 2015) and the high monsoonal runoff was observed from the Indus River during ~ 3.5–2.2 ka BP (von Rad et al. 1999). Similar situation was prevailed in the Garhwal Himalaya from ~ 3.5 to 1.8 ka BP (Kotlia and Joshi 2013) and in the central Ganga plain (Basaha lake) from 3.3 ka BP onwards (Chauhan et al. 2004). Our results support an evidence of restoration of mixed oak forest in response to amelioration of climate in the temperate zone of Kumaun Himalaya around 2.9 ka BP (Gupta 2008). However, all the records are expanded due to temporal resolution of different proxy and perhaps withdrawal of the monsoon seasonality with increased influence of WDs in NW Himalaya.

~ 2.7–1.5 ka BP (reduced precipitation) The TC1 records show climatic worsening from 2.7 ka BP onwards with two drought events at ~ 1.9 ~ 1.6 ka BP (Fig. 11). Similar fluctuations in stalagmite $\delta^{18}O$ were also observed from the Sainji cave, Kumaun Himalaya (Kotlia et al. 2015) between ~ 2.0 and 0.8 ka BP (Fig. 11). The trend of $\delta^{18}O$ value towards positive in Soreq cave within the period was characterized by gradual decrease in rainfall (Fig. 11; Bar-Matthews et al. 2003). The relatively dry periods were also documented from eastern Mediterranean after 1.9 ka (Orland et al. 2008). In general, the Dongge cave experienced reduced precipitation after 3.5 ka BP (Dykoski et al. 2005), while the higher amplitude peaks with increased values of $\delta^{18}O$ observed at ~ 2.1 and 1.8 ka BP can be equated with TC1 (Fig. 11) although Wang et al. (2005) noted the weakened intensity of monsoon at ~ 1.6 cal ka. A progressive lowering of Tso Moriri lake level from 2.7 ka BP onwards was also viewed by Mishra et al. (2015). Rühland et al. (2006) also pointed out the drier climatic conditions around 1.6 ka BP in the Pinder valley. Intensified glacier activity and cooler climate has been documented from Himalaya at ~ 2.0 ka BP (Chauhan 2003; Kar et al. 2002). Speleothem records from the Pokhara valley (Central Nepal) confirm the reduced monsoonal precipitation and increased aridity due to deposition of aragonite layers between 2.3 and 1.5 ka BP (Denniston 2000). Pollen data obtained from the Spiti region also specify cool/dry conditions between ~ 2.0 and 1.0 ka BP (Mazari et al. 1996) and a severe weakening of ISM activity around ~ 1.5 ka BP is evident in historical records from India (Pandey et al. 2003).

Conclusions

Variations in the TC1 $\delta^{18}O$ values primarily reflect the past precipitation variability. A positive relationship of $\delta^{18}O$ variations with previously established records of mid-late Holocene climatic variability shows that the ^{14}C AMS dates used in the young speleothems are expected realistic within the age uncertainties. Three major climatic phases are documented by studying the TC1 stalagmite: (1) declined precipitation between 4.0 and 3.4 ka BP, (2) gradual improvement in the climatic condition from 3.4 to 2.7 ka BP and (3) reduced precipitation conditions from ~ 2.7 until the end of TC1 deposition. During the last ~ 4.0 ka BP, we identified three dry events at ~ 3.5, ~ 1.9 and ~ 1.6 ka BP. The ~ 3.5 ka BP event is equated with transitions between mid and late Holocene and coincides with de-urbanization of the Indus valley civilization. Diversified records and large variations in speleothem $\delta^{18}O$ from a number of the northwest Himalayan areas indicate the relative contribution of WDs during the late Holocene, a topic which has not been much incited before.

Acknowledgements The study was funded under the SERB/DST Fast Track Scheme (Project No. SR SR/FTP/ES-91/2012) awarded to LMJ, and the MoES project (MoES/PO/Geosci/43/2015), executed by BSK. Our sincere thanks are due to Prof. Goslar for providing ^{14}C AMS dates. C.-C. Shen is grateful to Taiwan ROC MOST grants (103-2119-M-002-022 and 104-2119-M-002-003). We thank the Directors, JNCSAR, Bangalore and NGRI, Hyderabad for providing analytical facilities and CAS in Geology, Kumaun University, Nainital for working facilities. Thanks are also due to both anonymous reviewers for their valuable comments to enable us improve the manuscript.

References

Ahmad SM, Anil Babu G, Padmakumari VM, Waseem R (2008) Surface and deep water changes in the northeast Indian Ocean during the last 60 ka inferred from carbon and oxygen isotopes of planktonic and benthic foraminifera. Palaeogeogr Palaeoclimatol Palaeoecol 262: 182–188

Bar-Matthews M, Ayalon A, Kaufman A, Wasserburg GJ (1999) The Eastern Mediterranean paleoclimate as a reflection of regional events: Soreq cave, Israel. Earth Planet Sci Lett 166:85–95

Bar-Matthews M, Ayalon A, Gilmour M, Matthews A, Hawkesworth CJ (2003) Sea land oxygen isotopic relationships from planktonic foraminifera and speleothems in the Eastern Mediterranean region and their implication for paleorainfall during interglacial intervals. Geochim Cosmochim Acta 67(17):3181–3199

Benn DI, Owen LA (1998) The role of the Indian Summer Monsoon and the mid-latitude westerlies in Himalaya glaciation: review and speculative discussion. Journal of Geological Society, London 155:353–363

Bhargava ON, Frank W, Bertle R (2011) Late Cambrian deformation in the Lesser Himalaya. J Asian Earth Sci 40:201–212

Blyth AJ, Hua Q, Smith A, Frisia S, Borsato A, Hellstrom J (2017) Exploring the dating of "dirty" speleothems and cave sinters using radiocarbon dating of preserved organic matter. Quat Geochronol 39:92–98

Bronk Ramsey C (1995) Radiocarbon calibration and analysis of stratigraphy: the OxCal program. Radiocarbon 37(2):425–430

Bronk Ramsey C (2001) Development of the radiocarbon calibration program. Radiocarbon 43(2A):355–363

Bronk Ramsey C (2008) Deposition models for chronological records. Quat Sci Rev 27:42–60

Burns SJ, Matter A, Frank N, Mangini A (1998) Speleothem-based paleoclimate record from northern Oman. Geology 26(6):499–502

Burns SJ, Fleitmann D, Matter A, Neff U, Mangini A (2001) Speleothem evidence from Oman for continental pluvial events during interglacial periods. Geology 29:623–626

Burns SJ, Fleitmann D, Matter A, Kramers J, Al-Subbary AA (2003) Indian Ocean climate and an absolute chronology over Dansgaard/Oeschger events 9 to 13. Science 288:847–850

Chauhan OS (2003) Past 20,000-year history of Himalayan aridity: evidence from oxygen isotope records in the Bay of Bengal. Curr Sci 84(1):190–193

Chauhan MS, Sharma C (1996) Pollen analysis of mid-Holocene sediments from Kumaon Himalaya. Geol Surv India Spec Publ 21:257–269

Chauhan MS, Sharma C, Singh IB, Sharma S (2004) Proxy records of late Holocene vegetation and climate changes from Basaha Jheel, Central Ganga Plain. J Palaeontol Soc India 49:27–34

Cheng H, Edwards RL, Shen C-C, Polyak VJ, Asmerom Y, Woodhead J, Hellstrom J, Wang Y, Kong X, Spötl C (2012) Improvements in ^{230}Th dating, ^{230}Th and ^{234}U half-life values, and U–Th isotopic measurements by multi-collector inductively coupled plasma mass spectroscopy. Earth Planet Sci Lett 371-372:82–91

Dansgaard W (1964) Stable isotopes in precipitation. Tellus 16:436–468

Demske D, Tarasov PE, Leipe C, Kotlia BS, Joshi LM, Long T (2016) Record of vegetation, climate change, human impact and retting of hemp in Garhwal Himalaya (India) during the past 4600 years. The Holocene:1–15. doi:10.1177/0959683616650267

Denniston RF, Gonzalez LA, Asmerom Y, Sharma RH, Reagan MK (2000) Speleothem evidence for changes in Indian Summer Monsoon precipitation over the last 2300 years. Quat Res 53:196–202

Dixit Y, Hodell DA, Petrie CA (2014) Abrupt weakening of the summer monsoon in northwest India ~4100 yr ago. Geology 42(4):339–342

Dorale J, Liu Z (2009) Limitations of Hendy test criteria in judging the paleoclimatic suitability of speleothems and the need for replication. Journal of Cave and Karst Studies 71(1):73–80

Duan W, Kotlia BS, Tan M (2013) Mineral composition and structure of the stalagmite laminae from Chulerasim cave, Indian Himalaya and the significance for palaeoclimatic reconstruction. Quat Int 298:93–97

Durand N, Hamelin B, Deschamps P, Gunnell Y, Curmi P (2016) Systematics of U-Th disequilibrium in calcrete profiles: lessons from southwest India. Chem Geol 446:54–69

DyKoski C, Edwards RL, Cheng H, Yuan DX, Cai YJ, Zhang ML, Lin YS, Qing JM, An ZS, Revenaugh J (2005) A high resolution absolute dated Holocene and deglacial Asian monsoon record from Dongge cave, China. Earth Planet Sci Lett 233:71–86

Fleitmann D, Burns SJ, Neff U, Mudelsee M, Mangini A, Matter A (2004) Palaeoclimatic interpretation of high-resolution oxygen isotope profiles derived from annually laminated speleothems from Southern Oman. Quat Sci Rev 23:935–945

Fleitmann D, Burns SJ, Mangini A, Mudelsee M, Kramers J, Villa I, Neff U, Al-Subbary AA, Buettner A, Hippler D, Matter A (2007) Holocene ITCZ and Indian monsoon dynamics recorded in stalagmites from Oman and Yemen (Socotra). Quat Sci Rev 26:170–188

Garnett ER, Gilmour MA, Rowe PJ, Andrews JE, Preece RC (2004) ^{230}Th/^{234}U dating of Holocene tufas: possibilities and problems. Quat Sci Rev 23:947–958

Gasse F, Van Campo E (1994) Abrupt post glacial climate events in west Asia and North Africa monsoon domains. Earth Planet Sci Lett 126:435–456

Genty D, Massault M (1997) Bomb ^{14}C recorded in laminated speleothems—calculation of dead carbon proportion. Radiocarbon 39(1):33–48

Genty D, Baker A, Massault M, Proctor C, Gilmour M, Pons-Branchu E, Hamelin B (2001) Dead carbon in stalagmites: carbonate bedrock paleodissolution vs. ageing of soil organic matter. Implications for 13C variations in speleothems. Geochim Cosmochim Acta 65(20):3443–3457

Gonfiantini R, Roche MA, Olivry JC, Fontes JC, Zuppi GM (2001) The altitude effect on the isotopic composition of tropical rains. Chemical Geology 181:147–167

Goslar T, Hercman H, Pazdur A (2000) Comparison of U-series and radiocarbon dates of speleothems. Radiocarbon 42(3):403–414

Gupta A (2008) Late Quaternary vegetation and climate from temperate zone of the Kumaun Himalaya, India (with remarks on neotectonic disturbance). Acta Palaeobotanica 48(2):325–333

Gupta AK, Mohan K, Das M, Singh RK (2013) Solar forcing of the Indian summer monsoon variability during the Ållerød period. Sci Report 3:2753. doi:10.1038/srep02753

Hassan FA, Stucki BR (1987) Nile floods and climatic change. In: Rampino MR, Sanders JE, Newman WS, Konigsson LK (eds) Climate: history, periodicity and predictability. Van Nostrand Reinhold, New York, pp 37–46

Hendy CH (1971) The isotopic geochemistry of speleothems-I. The calculation of the effects of different modes of formation on the isotopic composition of speleothems and their applicability as paleoclimatic indicators. Geochimica et Cosmochimica Acta 35:801–824

Hercman H, Goslar T (2002) Uranium-series and radiocarbon dating of speleothems—methods and limitations. Acta Geol Pol 52(1):35–41

Hren MT, Bookhagen B, Blisniuk PM, Booth AL, Chamberlain CP (2009) δ18O and δD of streamwaters across the Himalaya and Tibetan Plateau: implications for moisture sources and paleoelevation reconstructions. Earth Planet Sci Lett 288:20–32

Hua Q, McDonald J, Redwood D, Drysdale R, Lee S, Fallon S, Hellstrom J (2012) Robust chronological reconstruction for young speleothems using radiocarbon. Quat Geochronol 14:67–80

Indian disaster report (2013) (http://nidm.gov.in/PDF/pubs/India%20Disaster%20Report % 202013.pdf)

Jaffey AH, Flynn KF, Glendenin LE, Bentley WC, Essling AM (1971) Precision measurement of half-lives and specific activities of U-235 and U-238. Physical Reviews 4:1889–1906

Joseph S, Sahai AK, Goswami BN (2009) Eastward propagating MJO during boreal summer and Indian monsoon droughts. Clim Dyn 32:1139–1153

Joshi LM, Kotlia BS (2015) Neotectonically triggered instability around the palaeolake regime in Central Kumaun Himalaya, India. Quat Int 371:219–231

Kar R, Ranhotra PS, Bhattacharyya A, Sekar B (2002) Vegetation vis-a-vis climate and glacial fluctuations of the Gangotri glacier since the last 2000 years. Curr Sci 82(3):347–351

Kotlia BS, Joshi LM (2013) Late Holocene climatic changes in Garhwal Himalaya. Curr Sci 104(7):911–919

Kotlia BS, Bhalla MS, Sharma C, Rajagopalan G, Ramesh R, Chauhan MS, Mathur PD, Bhandari S, Chacko ST (1997) Palaeoclimatic conditions in the upper Pleistocene and Holocene Bhimtal–Naukuchiatal lake basin in south central Kumaun, North India. Palaeogeogr Palaeoclimatol Palaeoecol 130:307–322

Kotlia BS, Sanwal J, Phartiyal B, Joshi LM, Trivedi A, Sharma C (2010) Late Quaternary climatic changes in the eastern Kumaun Himalaya, India, as deduced from multi-proxy studies. Quat Int 213:44–55

Kotlia BS, Ahmad SM, Zhao J-X, Raza W, Collerson KD, Joshi LM, Sanwal J (2012) Climatic fluctuations during the LIA and post-LIA in the Kumaun Lesser Himalaya, India: evidence from a 400 y old stalagmite record. Quat Int 263:129–138

Kotlia BS, Singh AK, Joshi LM, Dhaila BS (2015) Precipitation variability in the Indian Central Himalaya during last ca. 4,000 years inferred from a speleothem record: impact of Indian Summer Monsoon (ISM) and Westerlies. Quat Int 371:244–253

Kotlia BS, Singh AK, Zhao J-X, Duan W, Tan M, Sharma AK, Raza W (2017) Stalagmite based high resolution precipitation variability for past four centuries in the Indian Central Himalaya: Chulerasim cave re-visited and data re-interpretation. Quat Int 444:35–34

Kumar B, Rai SP, Kumar US, Verma SK, Garg P, Kumar SVV, Jaiswal R, Purendra BK, Kumar SR, Pande NG (2010) Isotopic characteristics of Indian precipitation. Water Resour Res 46:W12548. doi:10.1029/2009WR008532

Laskar AH, Raghav S, Yadava MG, Jani RA, Narayana AC, Ramesh R (2011) Potential of stable carbon and oxygen isotope variations of speleothems from Andaman Islands, India, for paleomonsoon reconstruction. J Geol Res. doi:10.1155/2011/272971

Laskar AH, Yadava MG, Ramesh R, Polyak VJ, Asmerom Y (2013) A 4 kyr stalagmite oxygen isotopic record of the past Indian Summer Monsoon in the Andaman Islands. Geochemistry Geophysics Geosystems 14(9):3555–3566

Lechleitner FA, Fohlmeister J, McIntyre C, Baldini LM, Jamieson RA, Hercman H, Gąsiorowski M, Pawlak J, Stefaniak K, Socha P (2016) A novel approach for construction of radiocarbon-based chronologies for speleothems. Quat Geochronol 35:54–66

Leipe C, Demske D, Tarasov PE and HIMPAC Project Members (2014) A Holocene pollen record from the northwestern Himalayan lake TsoMoriri: implications for palaeoclimatic and archaeological research. Quat Int 348:93–112

Li H, Ku T-L, Chen W, Jiao W, Zhao S, Chen T, Li T (1996) Isotope studies of Shihua Cave, Beijing (II): radiocarbon dating and age correction of stalagmite. Seismology and Geology 18(4):329–338

Liang F, Brook GA, Kotlia BS, Railsback LB, Hardt B, Cheng H, Edwards RL, Kandasamy S (2015) Panigarh cave stalagmite evidence of climate change in the Indian Central Himalaya since AD 1256: monsoon breaks and winter southern jet depressions. Quat Sci Rev 124:145–161

Lone MA, Ahmad SM, Dung NC, Shen CC, Raza W, Kumar A (2014) Speleothem based 1000-year high resolution record of Indian monsoon variability during the last deglaciation. Palaeogeogr Palaeoclimatol Palaeoecol 395:1–8

Mattey D, Lowry D, Duffet J, Fisher R, Hodge E, Frisia S (2008) A 53 year seasonally resolved oxygen and carbon isotope record from a modern Gibraltar speleothem: reconstructed drip water and relationship to local precipitation. Earth Planet Sci Lett 269:80–95

Mazari RK, Bagati TN, Chauhan MS, Rajagopalan G (1996) Palaeoclimatic record of last 2000 years in trans-Himalayan Lahaul-Spiti region. Proceedings of Nagoya IGBP-PAGES/PEP-II Symposium, In, pp 262–269

Mishra PK, Anoop A, Schettler G, Prasad S, Jehangir A, Menzel P, Naumann R, Yousuf AR, Basavaiah N, Deenadayalan K, Wiesner MG, Gaye B (2015) Reconstructed late Quaternary hydrological changes from Lake Tso Moriri, NW Himalaya. Quat Int 371:76–86

Neff U, Burns SJ, Mangini A, Mudelsee M, Fleitmann D, Matter A (2001) Strong coherence between solar variability and the monsoon in Oman between 9 and 6 kyr ago. Nature 411:290–293

Orland IJ, Bar-Matthews M, Kita NT, Ayalon A, Matthews A, Valley JW (2008) Climate deterioration in the eastern Mediterranean as revealed by ion microprobe analysis of a speleothem that grew from 2.2 to 0.9 ka in Soreq Cave, Israel. Quat Res 71:27–35

Pandey DN, Gupta AK, Anderson DM (2003) Rainwater harvesting as an adaptation to climate change. Curr Sci 85:46–59

Pant GB (2003) Long- term climate variability and change over monsoon Asia. Journal of Indian Geophysical Union 7(3):125–134

Perrin C, Prestimonaco L, Servelle G, Tilhac R, Maury M, Cabrol P (2014) Aragonite–calcite speleothems: identifying original and diagenetic features. J Sediment Res 84:245–269

Phadtare NR (2000) Sharp decrease in summer monsoon strength 4000e3500 cal yr BP in the Central Higher Himalaya of India based on pollen evidence from alpine peat. Quat Res 53:122–129

Rawat S, Gupta AK, Sangode SJ, Srivastava P, Nainwal HC (2015) Late Pleistocene–Holocene vegetation and Indian summer monsoon record from the Lahaul, northwest Himalaya, India. Quaternary Science Review 114:167–181

Ray PK, Chattoraj CSL, Bisht MPS, Kannaujiya S, Pandey K, Goswami A (2016) Kedarnath disaster 2013: causes and consequences using remote sensing inputs. Nat Hazards 81(1):227–243

Raza W, Ahmad SM, Lone MA, Shen, CC, Sarma DS, Kumar A (2017) Summer monsoon variability in southern India during the last deglaciation: evidence from a high resolution stalagmite $\delta^{18}O$ record. Palaeogeogr Palaeoclimatol Palaeoecol doi 10.1016/j.palaeo.2017.07.003

Rehfeld K, Marwan N, Breitenbach SFM, Kurths J (2012) Late Holocene Asian summer monsoon dynamics from small but complex networks of paleoclimate data. Clim Dyn 41(1):3–19

Reimer PJ, Bard E, Bayliss A, Beck JW, Blackwell PG, Bronk Ramsey C, Buck CE, Cheng H, Edwards RL, Friedrich M, Grootes PM, Guilderson TP, Haflidason H, Hajdas I, Hatté C, Heaton TJ, Hoffmann DL, Hogg AG, Hughen KA, Kaiser KF, Kromer B, Manning SW, Niu M, Reimer RW, Richards DA, Scott EM, Southon JR, Staff RA, Turney CSM, van der Plicht J (2013) IntCal13 and Marine13 radiocarbon age calibration curves 0–50,000 years cal BP. Radiocarbon 55(4):1869–1887

Rozanski K, Araguas-Araguas L, Gonfiantini R (1992) Relation between long term trends of oxygen-18 isotope composition of precipitation and climate. Science 258:981–985

Rühland K, Phadtare NR, Pant RK, Sangode SJ, Smol JP (2006) Accelerated melting of Himalayan snow and ice triggers pronounced changes in a valley peat land from northern India. Geophys Res Lett 33:L15709. doi:10.1029/2006GL026704

Sanwal J, Kotlia BS, Rajendran C, Ahmad SM, Rajendran K, Sandiford M (2013) Climatic variability in central Indian Himalaya during the last 1800 years: evidence from a high resolution speleothem record. Quat Int 304:183–192

Scholz D, Hoffmann DL, Hellstrom J, Bronk Ramsey C (2012) A comparison of different methods for speleothem age modelling. Quat Geochronol 14:94–104

Sharma S, Joachimski M, Sharma M, Tobschall HJ, Singh IB, Sharma C, Chauhan MS, Morgenorth G (2004) Late glacial and Holocene environmental changes in Ganga Plain, Northern India. Quat Sci Rev 23:145–159

Shen CC, Cheng H, Edwards RL, Moran SB, Edmonds HN, Hoff JA, Thomas RB (2003) Measurement of attogram quantities of 231Pa in dissolved and particulate fractions of seawater by isotope dilution thermal ionization mass spectroscopy. Anal Chem 75:1075–1079

Shen CC, Wu CC, Cheng H, Edwards RL, Hsieh YT, Gallet S, Chang CC, Li TY, Lam DD, Kano A, Hori M, Spötl C (2012) High-precision and high-resolution carbonate ^{230}Th dating by MC-ICP-MS with SEM protocols. Geochim Cosmochim Acta 99:71–86

Sinha A, Cannariato KG, Stott LD, Li HC, You CF, Cheng H, Edwards RL, Singh IB (2005) Variability of Southwest Indian summer monsoon precipitation during the Bølling-Ållerød. Geology 33:813–816

Sinha A, Cannariato KG, Stott LD, Cheng H, Edwards RL, Yadava MG, Ramesh R, Singh IB (2007) A 900-year (600 to 1500 A.D.) record of the Indian summer monsoon precipitation from the core monsoon zone of India. Geophysical Research Letters 34:L16707. doi:10.1029/2007GL030431

Sinha A, Kathayat G, Cheng H, Breitenbach SFM, Berkelhammer M, Mudelsee M, Biswas J, Edwards RL (2015) Trends and oscillations in the Indian summer monsoon rainfall over the last two millennia. Nat Commun 6:6309. doi:10.1038/ncomms7309

Smith BN (1972) Natural abundance of the stable isotopes of carbon in biological systems. Bioscience 22:226–231

Smith BN, Epstein S (1971) Two categories of 13C/12C ratios for higher plants. Plant Physiol 47:380–284

Thakur VC, Rawat BS (1992) Geologic map of western Himalaya, 1:1, 000,000. India, Wadia Institute of Himalayan Geology, Dehra Dun

von Rad U, Schulz H, Riech V, den Dulk M, Berner U, Sirocko F (1999) Multiple monsoon-controlled breakdown of oxygen-minimum conditions during the past 30,000 years documented in laminated sediments off Pakistan. Palaeogeogr Palaeoclimatol Palaeoecol 152(1): 129–161

Wang Y, Cheng H, Edwards RL, He Y, Kong X, An Z, Wu J, Kelly MJ, Dykoski CA, Li X (2005) The Holocene Asian Monsoon: links to solar changes and North Atlantic climate. Science 308(5723):854–857

Webster PJ (1987) The elementary monsoon. In: Fein JS, Stephens PL (eds) Monsoons. Wiley, New York, pp 3–32

Webster PJ, Magana VO, Palmer TN, Shukla J, Tomas RA, Yanai M, Yasunari T (1998) Monsoons: processes, predictability, and the prospects for prediction. J Geophys Res 103(C7):14451–14510

Weiss H, Coutry MA, Wetterstrom W, Guichard F, Senior L, Meadow R, Curnow A (1993) The genesis and collapse of third millennium north Mesopotamian civilization. Science 261:995–1004

Winner C (2012) Rain, rivers, and the fate of civilizations. Oceanus Magazine 49(3):30

Wright RP (2010) The ancient Indus: urbanism, economy and society: case studies in early societies, vol 10. Cambridge University Press, Cambridge UK, p 416

Xiao X, Haberle SG, Shen J, Yang X, Han Y, Zhang E, Wang S (2014) Latest Pleistocene and Holocene vegetation and climate history inferred from an alpine lacustrine record, northwestern Yunnan Province, southwestern China. Quat Sci Rev 86:35–48

Yadava MG, Ramesh R (2005) Monsoon reconstruction from radiocarbon dated tropical Indian Speleothem. The Holocene 15:48–59

Yadava MG, Ramesh R, Pant GB (2004) Past monsoon rainfall variations in peninsular India recorded in a 331-year-old speleothem. The Holocene 14:517–524

Zhao M, Li HC, Liu ZH, Mii HS, Sun HL, Shen CC, Kang SC (2015) Changes in climate and vegetation of central Guizhou in southwest China since the last glacial reflected by stalagmite records from Yelang Cave. J Asian Earth Sci 114(3):549–561

Zhou HY, Zhao JX, Wang Q, Feng YX, Tang J (2011) Speleothem-derived Asian summer monsoon variations in Central China during 54–46 ka. J Quat Sci 26(8):781–790. doi:10.1002/jqs.1506